Effect of substrate clamping on evolution of properties in homovalent and heterovalent relaxor thin films

Zishen Tian,[1] Jieun Kim,[1] Abel Fernandez,[1] Xiaoxi Huang,[1] and Lane W. Martin[1,2,*]

[1]*Department of Materials Science and Engineering, University of California, Berkeley, Berkeley, California 94720, USA*

[2]*Materials Sciences Division, Lawrence Berkeley National Laboratory, Berkeley, California 94720, USA*

(Received 18 June 2021; revised 10 February 2022; accepted 11 February 2022; published 11 March 2022)

Relaxor ferroelectrics, well known for their large dielectric and piezoelectric response, are attracting growing interest in thin-film form driven by a need for miniaturized devices. Fundamental understanding and control of the performance of relaxors as thin films, however, is underdeveloped relative to studies of bulk versions. One obvious challenge is substrate clamping, which reduces the dielectric and piezoelectric response, yet systematic comparisons of the effect of substrate clamping on different relaxor materials is missing. Here, the impact of epitaxial constraint on the relaxor behavior and properties of both homovalent $BaZr_{0.5}Ti_{0.5}O_3$ and heterovalent $PbMg_{1/3}Nb_{2/3}O_3$ relaxors is studied in (001)-, (011)-, and (111)-oriented thin films. While the different orientations of $PbMg_{1/3}Nb_{2/3}O_3$ heterostructures show little variation in dielectric permittivity, a strong orientational effect is observed in $BaZr_{0.5}Ti_{0.5}O_3$ heterostructures, with (111)-oriented films exhibiting a 67% higher dielectric permittivity than (001)-oriented films, a difference that is attributed to how substrate clamping along different crystallographic axes interacts with the polar-structure nucleation and growth. Measurements of dielectric anisotropy in (001)-oriented films confirm the trend—with $PbMg_{1/3}Nb_{2/3}O_3$ heterostructures exhibiting just half as much anisotropy in dielectric permittivity than $BaZr_{0.5}Ti_{0.5}O_3$ heterostructures. These results indicate a higher susceptibility to substrate clamping in homovalent relaxors as compared to heterovalent relaxors, implying that the random fields in the heterovalent relaxors could be advantageous for materials in such geometries and applications.

DOI: 10.1103/PhysRevB.105.094107

I. INTRODUCTION

Relaxor ferroelectrics, especially perovskite oxides such as $(1-x)PbMg_{1/3}Nb_{2/3}O_{3-}(x)PbTiO_3$ (PMN-PT), are widely studied due to their large piezoelectric, dielectric, and pyroelectric response and potential for use in applications ranging from motors, sensors, and energy harvesters [1,2], to capacitive energy storage [3,4], waste-heat scavenging [5], and electrocaloric cooling [6,7]. Such applications are, in turn, increasingly driving research to consider not just bulk ceramic and single-crystal versions, but also thin-film geometries. The move to thin films allows for both the miniaturization of devices [8] and a reduction in the voltages required to achieve a desired effect (e.g., strain-mediated magnetoelectric coupling) [3–7,9]. There are, however, a number of factors that can limit the performance of relaxor thin films including size effects [10], imprint [11], and substrate-induced clamping [12–14]. Clamping, wherein a thin film is mechanically restricted by its connection to a semi-infinite, rigid substrate, can dramatically limit dielectric and piezoelectric response. Attempts to alleviate substrate clamping include fabricating films into strips or islands [13–15] and releasing the film from the substrate [16–18]. While researchers have sought innovative ways to address this challenge, less effort has been placed on understanding if substrate clamping affects all relaxors in the same way; in essence asking are all relaxors equally good (or bad) for use in thin-film devices?

Relaxors can be classified based on the physical origin of the short-range interactions which shape their microscopic structures. While the exact microscopic structure of relaxors is still a matter of ongoing discussion [19], the general consensus is that the presence of either polar nanoregions (PNRs) [20,21] embedded in a nonpolar matrix or polar nanodomains (PNDs) [22] separated by low-angle domain walls are critical to the interesting response. Here, we will refer to them as nanoscale-polar structures. It is believed that the long-range polar order in these materials is broken by short-range interactions [23], which are either elastic, electric, or a combination of both in origin [24]. In homovalent relaxors such as $BaZr_{0.5}Ti_{0.5}O_3$ (BZT), the *B*-site cations (Zr^{4+} and Ti^{4+}) are the same valence but differ in size (Zr^{4+} and Ti^{4+} have ionic radii of 72 and 60.5 pm, respectively). Thus, a random distribution of these *B*-site cations generates a random elastic field [25]. In heterovalent relaxors such as $PbMg_{1/3}Nb_{2/3}O_3$ (PMN), on the other hand, the *B*-site cations differ in both valence and size (Mg^{2+} and Nb^{5+} have ionic radii of 72 and 64 pm, respectively) giving rise to both elastic and electric random fields. Under an applied electric field, the random electric field can be suppressed, and a long-range ordered polar phase can arise from the percolating growth of large domains [23], or alternatively from the alignment of nanoscale-polar structures [26]. If the random field is purely elastic in nature, however, the relaxor phase is relatively

*lwmartin@berkeley.edu

stable under applied electric fields [27]. While PMN shows a relaxor-to-ferroelectric phase transition in field-cooling experiments under an electric field of ∼3 kV/cm (along the [111]) [26], a similar phase transition in BZT has not been observed experimentally [28,29] and simulations predict the threshold field for such a transition to be ∼1000 kV/cm [30]. Thus, the random-field mechanism in a relaxor determines the stability of the relaxor phase under applied electric fields. Besides the random-field characteristics of the relaxor material, the crystal orientation is another important factor that determines the evolution of the polar order under external fields. For example, in PMN, the electric-field-induced relaxor-to-ferroelectric phase transition shows a strong orientation dependence. (111)-oriented crystals show a first-order transition and the lowest threshold field while a smooth transition is observed in (001)-oriented crystals [31]. As the polar structures are rhombohedral in local symmetry [32], the field applied along the polar [111] axis readily induces cooperative ordering of the dipoles.

Thus, in this work, we aim to understand how different types of relaxors (namely homovalent and heterovalent) and different orientations of those relaxors respond under substrate clamping. In essence, can (some of) the negative effects of clamping be ameliorated by proper choice and design of the relaxor material itself? Here, we report a comparison between (001)-, (011)-, and (111)-oriented thin films of homovalent BZT and heterovalent PMN relaxors grown via pulsed-laser deposition. Note that we chose PMN over PMN-PT, because PMN-PT transitions into low-symmetry phases upon cooling down, while PMN and BZT remain cubic, allowing a direct comparison between these two materials. Single-phase, epitaxial, and fully relaxed films of the relaxor materials were produced in all cases. The out-of-plane dielectric permittivity of each heterostructure type was measured as a function of frequency, temperature, AC-field amplitude, and DC field. While the different orientations of PMN heterostructures show little variation in critical temperatures and dielectric permittivity, a strong orientational effect is observed in the BZT heterostructures; with (111)-oriented films exhibiting a 67% higher dielectric permittivity, 25 K higher dielectric maximum temperature (T_m), and 70 K higher Burns temperature (T_B) as compared to (001)-oriented films. Analysis of possible dielectric contributions suggests that in BZT, changing the crystallographic axes along which the material is clamped results in a difference in the nucleation, growth, and interaction strength of the nanoscale-polar structures. Measurements of dielectric anisotropy in (001)-oriented heterostructures confirm these trends—with PMN heterostructures exhibiting just half as much anisotropy in dielectric permittivity as compared to the BZT heterostructures. These results indicate a lower susceptibility to substrate clamping in heterovalent relaxors as compared to homovalent relaxors, implying that the random fields in heterovalent relaxors could be advantageous for thin-film applications.

II. EXPERIMENT

Here, we study 75 nm $Ba_{0.5}Sr_{0.5}RuO_3$/100 nm $PbMg_{1/3}Nb_{2/3}O_3$ (PMN)/50 nm $Ba_{0.5}Sr_{0.5}RuO_3$ heterostructures and 75 nm $La_{0.7}Sr_{0.3}MnO_3$/100 nm $BaZr_{0.5}Ti_{0.5}O_3$ (BZT)/50 nm $La_{0.7}Sr_{0.3}MnO_3$ heterostructures deposited on $(LaAlO_3)_{0.3}$-$(Sr_2AlTaO_6)_{0.7}$ (LSAT) (001), (011), and (111) substrates (CrysTec GmbH) via pulsed-laser deposition in an on-axis geometry (5.5-cm target-to-substrate spacing), using a KrF excimer laser (248-nm wavelength, LPX-300, Coherent). $Ba_{0.5}Sr_{0.5}RuO_3$ bottom electrodes were deposited from a ceramic target of the same chemistry (Praxair) at a heater temperature of 750 °C in a dynamic oxygen pressure of 20 mTorr with a laser fluence of 2.0 J cm^{-2} (4-Hz laser repetition rate). $PbMg_{1/3}Nb_{2/3}O_3$ films were deposited from a ceramic target with 10% lead excess at a heater temperature of 600 °C in a dynamic oxygen pressure of 200 mTorr with a laser fluence of 1.8 J cm^{-2} (2-Hz laser repetition rate). Following the growth of the films, 75-nm $Ba_{0.5}Sr_{0.5}RuO_3$ top electrodes were deposited *in situ*, at the same conditions as the bottom electrodes but at a heater temperature of 600 °C, to avoid lead loss. For the BZT samples, $La_{0.7}Sr_{0.3}MnO_3$ bottom electrodes were deposited from a ceramic target of the same chemistry (Praxair) at a heater temperature of 700 °C in a dynamic oxygen pressure of 200 mTorr with a laser fluence of 1.45 J cm^{-2} (4-Hz laser repetition rate). $BaZr_{0.5}Ti_{0.5}O_3$ films were deposited from a ceramic target of the same chemistry at a heater temperature of 680 °C in a dynamic oxygen pressure of 20 mTorr with a laser fluence of 1.8 Jcm^{-2} (2-Hz laser repetition rate). Following the growth of the films, 75-nm $La_{0.7}Sr_{0.3}MnO_3$ top electrodes were deposited *in situ*, at the same conditions as the bottom electrodes. After the growth of the trilayer heterostructures, all samples were cooled to room temperature at 5 °C min^{-1} in a static oxygen pressure of 700 Torr. The crystal structures of all samples were characterized by x-ray diffraction studies. X-ray θ-2θ line scans, rocking curves, and reciprocal space mapping studies were measured with copper K_α radiation (X'Pert 3 MRD, PANalytical).

Circular capacitors were fabricated for out-of-plane dielectric permittivity and polarization-electric field hysteresis-loop measurements. After the growth of the heterostructures, the top electrodes were patterned into arrays of circular capacitors (25 μm in diameter) by ion milling (300 V beam voltage, 45 V acceleration voltage, 5 mA beam current, ∼8 nm min^{-1} milling rate). The ion milling was stopped after 10 minutes (or an 80 nm milling depth) to leave the films and the bottom electrodes intact. Interdigitated electrodes (IDEs) were fabricated for in-plane dielectric permittivity measurements. Instead of trilayer heterostructures, single-layer relaxor films were grown for this purpose. Specifically, 100-nm-thick PMN or BZT thin films were deposited on LSAT (001) substrates, using the same growth conditions as described above. After the growth, IDEs (8-μm finger spacing, 8-μm finger width, 500 μm finger length) were fabricated by room-temperature sputter deposition of a 50-nm-thick layer of platinum.

Dielectric permittivity and loss tangent were measured using an impedance analyzer (E4990A, Keysight Technologies). Temperature-dependent dielectric measurements were carried out in a cryogenic vacuum probe station (TTPX, Lake Shore Cryotronics, Inc.) across a temperature range from 83 to 573 K. Out-of-plane measurements were performed using an AC drive voltage of 5 mV (0.5 kV/cm) and completed across the frequency range 1–100 kHz, while in-plane measurements were conducted using an AC drive voltage of

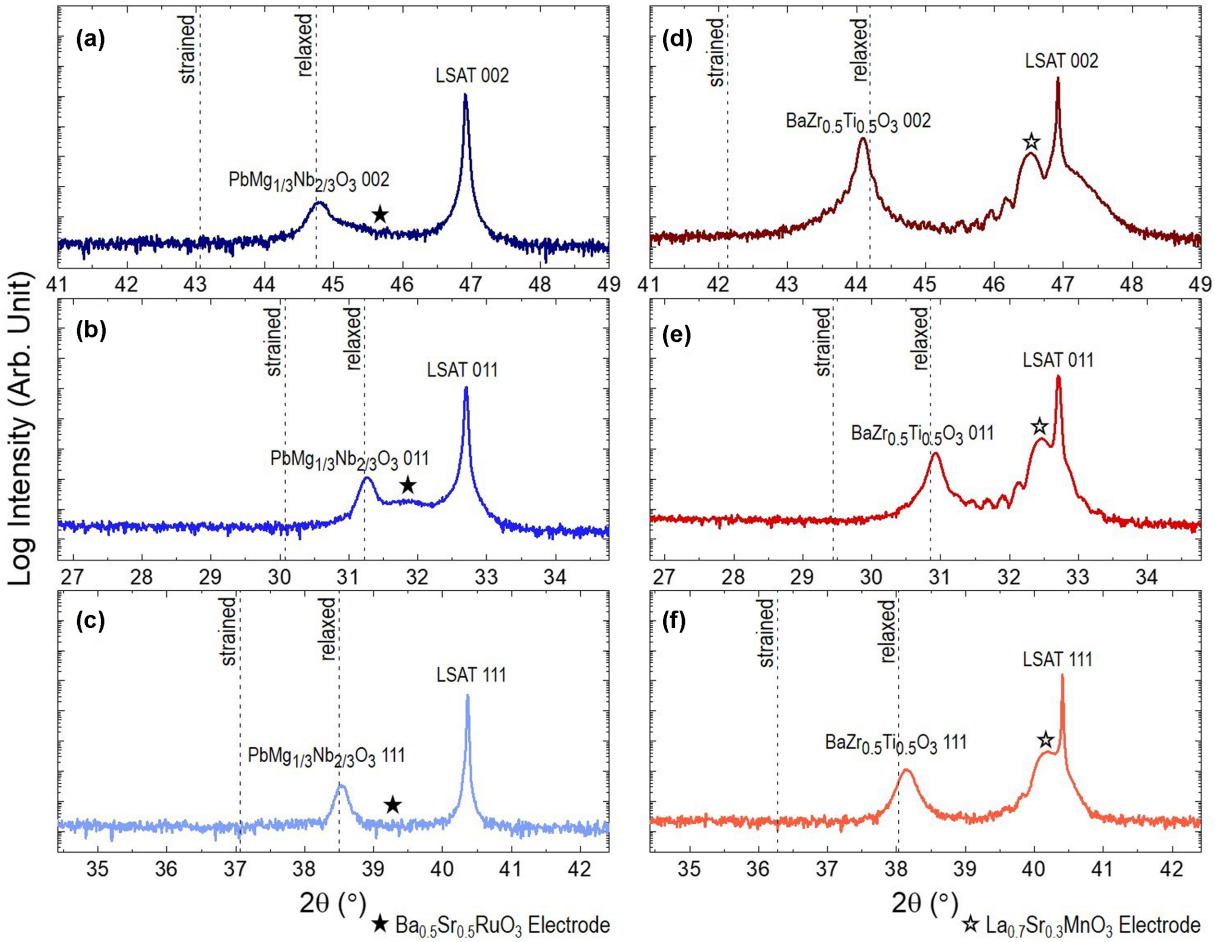

FIG. 1. X-ray θ-2θ line scans for the (a) (001)-, (b) (011)-, and (c) (111)-oriented $PbMg_{1/3}Nb_{2/3}O_3$ (PMN) heterostructures, and for the (d) (001)-, (e) (011)-, and (f) (111)-oriented $BaZr_{0.5}Ti_{0.5}O_3$ (BZT) heterostructures. Dashed lines show the expected peak positions for fully relaxed and fully strained versions of the films. Black (open) stars mark the expected peak positions for the $Ba_{0.5}Sr_{0.5}RuO_3$ ($La_{0.7}Sr_{0.3}MnO_3$) electrodes.

400 mV (0.5 kV/cm) to maintain the same field strength. Next, AC-field-dependent dielectric measurements were performed with an AC drive voltage of 5 mV–1 V (0.5–100 kV/cm) at a constant frequency of 10 kHz. Finally, DC-field-dependent measurements were carried out using an AC drive voltage of 5 mV (0.5 kV/cm) at 10 kHz with a DC bias voltage sweeping between ±5 V (±500 kV/cm). Polarization-electric field hysteresis loops were measured using a Precision Multiferroic Tester (Radiant Technologies), with a fixed frequency of 10 kHz and a temperature range of 78–298 K.

III. RESULTS AND DISCUSSION

X-ray diffraction studies were carried out on all six heterostructure variants and confirmed that all films are single phase and fully epitaxial (Fig. 1 and Supplemental Material, Figs. S1(a)–S1(f) [33]). Analysis of the full width at half maximum about the 002-, 011-, and 111-diffraction conditions of the PMN and BZT films grown on (001)-, (110)-, and (111)-oriented substrates, respectively, reveals that all three orientations of PMN heterostructures have nearly identical quality and mosaicity, but that the (001)- and (011)-oriented BZT films have considerably higher crystalline quality and smaller mosaicity than the (111)-oriented films (Supplemental Material, Figs. S1(g)–S1(i) [33]). Despite this observation, the crystalline quality is found to be irrelevant to the dielectric properties (Supplemental Material [33]). The lattice parameters of all films were extracted via x-ray reciprocal space mapping studies (Supplemental Material, Figs. S2 and S3 [33]) and the relaxor films were found to exhibit cubic structures in all cases, consistent with bulk versions [21,34]. Note that the local symmetry of the nanoscale-polar structures might be different from the average symmetry of the material, such as the tetragonal nanoscale-polar structures embedded in the monoclinic phase of PMN-PT [35,36], and the rhombohedral nanoscale-polar structures in the cubic phase of PMN and BZT [37,38]. The overall cubic structure is thus an average of the different variants of the local symmetries and does not indicate a paraelectric phase. The fact that no lattice distortion was observed in these films as compared to bulk versions indicates that all the films are in a relaxed-strain state, which can be attributed to the large lattice mismatch between the films and the LSAT substrate (lattice mismatch of −4.4% with PMN and −5.5% with BZT). Therefore, strain is not considered to be a dominant factor in these heterostructures, and thus the major variable at play here is the film orientation.

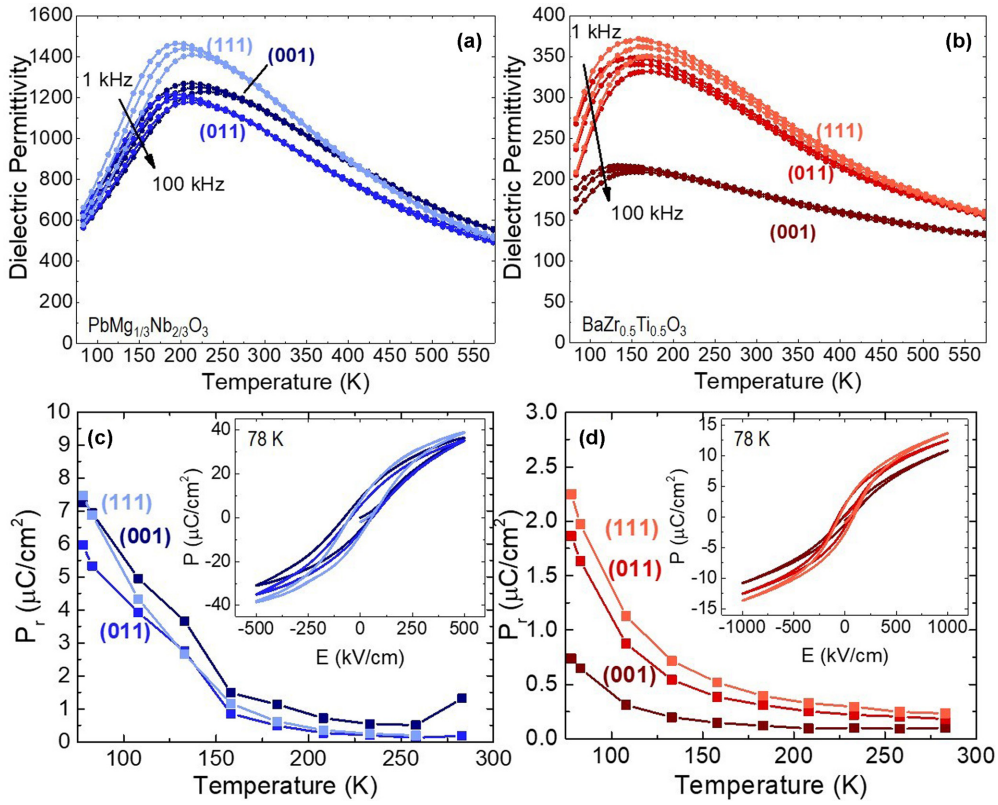

FIG. 2. Out-of-plane dielectric and ferroelectric measurements for clamped relaxor thin films. Dielectric permittivity as a function of temperature for (a) PMN and (b) BZT heterostructures at three different driving frequencies (1, 10, and 100 kHz). Temperature evolution of remnant polarization extracted from polarization-electric field hysteresis loops (insets show data at 78 K) for the (c) PMN and (d) BZT heterostructures. All hysteresis loops were measured at 10 kHz.

Thus, these heterostructures serve as a model set to explore the orientation-dependent clamping effect in both heterovalent and homovalent relaxors.

To compare the differently oriented heterostructures for the effects of substrate clamping, out-of-plane dielectric permittivity [Figs. 2(a) and 2(b)] and loss (Supplemental Material, Fig. S4 [33]) were measured as a function of frequency and temperature. The dielectric permittivity-temperature curves of all heterostructures show a broad peak with strong frequency dispersion, with T_m shifting with frequency, confirming the existence of a relaxor phase in all heterostructure variants [21]. While the PMN heterostructures [Fig. 2(a)] exhibit only a small orientation dependence with the percentage difference less than 22%, comparison of the different BZT heterostructures [Fig. 2(b)] reveals significant orientation dependence—with the (111)-oriented heterostructures showing a 67% higher dielectric response as compared to the (001)-oriented heterostructures at their dielectric peaks, indicating a stronger effect from clamping.

The critical temperatures for the relaxor films (Table I) were extracted from linear fits of the inverse dielectric constant-temperature plots (Supplemental Material, Fig. S5 [33]). The temperature where the curve deviates from the Curie-Weiss law is identified as T_B [39] and signifies the correlation of dipoles and the formation of "dynamic" nanoscale-polar structures. Below T_B, with another linear fit, the temperature of deviation is identified as the "intermediate" temperature T^* [40,41] and indicates the emergence of "static" nanoscale-polar structures. As the temperature drops further, the dynamics of the nanoscale-polar structures continuously slow [20,42]. Below T_m, the relaxation time of the nanoscale-polar structures surpasses the period of the probing electric field; thus, the dielectric response declines. All orientations of PMN heterostructures show similar critical temperatures within a span of 20 K, while the BZT heterostructures exhibit a strong orientation dependence wherein the (111)-oriented heterostructures have a T_B that is 70 K higher and a T_m which is 25 K higher (at 1 kHz) compared to the (001)-oriented heterostructures. This suggests that substrate clamping in the (111)-oriented heterostructures stabilizes the nanoscale-polar structures at higher

TABLE I. Summary of critical temperatures extracted from out-of-plane dielectric measurements (Figs. 2(a) and 2(b) and Supplemental Material, Fig. S5 [33]).

	T_m (1 kHz) K	ΔT_m (1–100 kHz) K	T^* K	T_B K
PMN (001)	213	20	353	453
PMN (011)	193	20	343	433
PMN (111)	193	20	353	443
BZT (001)	133	20	213	283
BZT (011)	153	20	253	303
BZT (111)	158	15	303	353

temperatures and exerts a stronger restraint to their reorientation. It should be noted that the increasing thermal stability of nanoscale-polar structures from (001)- to (111)-oriented films is consistent with the increasing dielectric permittivity, considering that the nanoscale-polar structures play a key role in the dielectric response of relaxors [19,43]. The smaller orientational difference of dielectric permittivity above T_B [Fig. 2(b)], in the absence of nanoscale-polar structures, also supports the relevance of nanoscale-polar structure response. Ultimately, these data show that substrate clamping along different crystallographic axes affects the polar structures and thus the dielectric response in BZT, yet the effect is weaker in PMN.

Further investigation of the orientational differences was conducted by measuring polarization-electric field hysteresis loops across a wide temperature range (Supplemental Material, Fig. S6 [33]). To shed light on the collective response of the frozen nanoscale-polar structures, we compared the polarization-electric field hysteresis loops at 78 K [insets, Figs. 2(c) and 2(d)]. The measurement was carried out at a sufficiently low temperature in attempt to frustrate the individual reorientation of nanoscale-polar structures to the most extent. An increasing trend of saturation polarization P_s from (001)- to (011)- to (111)-oriented heterostructures was observed in both the PMN and BZT heterostructures—consistent with that observed in PMN-PT single-crystal studies [2]—and attesting to the rhombohedral local symmetry in both PMN [32] and BZT [38]. The remnant polarization P_r is significantly reduced from the saturation polarization P_s as a result of the reorientation of the nanoscale-polar structures and thus indicates a large portion of nanoscale-polar structures are not frozen (even at this low temperature). Slim, relaxorlike hysteresis loops imply an absence of a relaxor-to-ferroelectric transition despite the low temperature and high applied electric fields ($\geqslant$500 kV/cm). This observation is consistent with studies for bulk versions of BZT [28,29], but not for bulk versions of PMN, where the nanoscale-polar structures freeze and the relaxor-to-ferroelectric transition occurs at ~220 K [26]. To study the temperature evolution of the nanoscale-polar structures, the P_r values were extracted as a function of temperature and compared among the different heterostructure variants [Figs. 2(c) and 2(d)]. Again, all PMN heterostructures reveal similar temperature evolution of the P_r. The BZT heterostructures again show orientation dependence with the (111)-oriented films exhibiting an elevated temperature for the onset of significant remnant polarization ($>0.25\,\mu C/cm^2$) compared to (001)-oriented films (233 K versus 108 K, respectively) and enhanced P_r values ($2.25\,\mu C/cm^2$ versus $0.73\,\mu C/cm^2$, respectively, at 78 K). As a fingerprint of the slow, nearly frozen nanoscale-polar structures, the onset of hysteresis manifests as an indicator of strong correlation between nearby nanoscale-polar structures and frustration of their individual reorientation. The observed orientational difference in the temperature evolution of P_r thus supports the difference in critical temperatures, attesting to stronger interactions and slower dynamics of nanoscale-polar structures in (111)- versus (001)-oriented clamped BZT heterostructures. This indicates that substrate clamping along the polar axis reinforces the interaction between the nanoscale-polar structures, with a more significant effect in the homovalent relaxor BZT than in the heterovalent relaxor PMN.

Understanding of the orientation dependence requires a detailed analysis of the different contributions to the dielectric response [19,43]. In relaxors, the dielectric response can be separated into that from the nanoscale-polar-structure and background contributions. The former includes both reorientation of the polar structures [44] and oscillation of domain walls [45], while the latter can be understood as either the paraelectric-matrix contribution (in the PNR picture) or the stationary-domain contribution [22,46] (in the PND picture). Under a sufficiently high DC bias the nanoscale-polar structure contribution can be completely suppressed, while the background contribution remains partially active. In studies of the dielectric permittivity as a function of background DC electric field [Figs. 3(a) and 3(b)], the permittivity of the (001)- and (111)-oriented PMN heterostructures are tuned by a similar percentage (68% versus 73%, respectively, under $500\,kV\,cm^{-1}$), while the (001)- and (111)-oriented BZT heterostructures exhibit a larger difference in the tunable part (42% versus 61%, respectively, under $500\,kV\,cm^{-1}$). It is further noted that the orientational difference in both the PMN and BZT heterostructures diminishes under high bias fields, indicating an absence of orientation dependence for the background contribution. Thus, the enhanced tunability in the (111)-oriented BZT heterostructure suggests the existence of a strong nanoscale-polar structure contribution.

To evaluate the relative importance of reorientations and domain-wall oscillations in constituting the nanoscale-polar structure contribution to the dielectric response, additional analysis was performed based on AC field-dependent dielectric measurements. Here, we show (111)-oriented PMN and BZT heterostructures as typical examples [Figs. 3(c) and 3(d)], but the (001)- and (011)-oriented heterostructures exhibit similar behaviors (Supplemental Material, Fig. S7 [33]). At 83 K, the dielectric permittivity is enhanced by increasing the AC field, which indicates that the mechanism for dielectric response requires activation, as is typical for domain-wall motion [47,48]. The strong interaction of the nanoscale-polar structures restrains the individual reorientation of the polar structures, and the domain-wall response dominates. At 183 K, the required activation for maximum dielectric response decreases, as evidenced by the peak in response moving from >100 to 35 kV/cm (33 kV/cm) for PMN (BZT) and the peak value reducing from >1.99 to 1.06 (>1.24 to 1.03) for PMN (BZT). The required activation further decreases as temperature increases. At 383 K, the AC field dependence vanishes, which is consistent with an absence of domain-wall response. It is noted that this temperature is above the T^* of all heterostructure variants (Table I), where the nanoscale-polar structures become dynamic and transient; hence, the interaction is weak and free reorientation dominates. We also compared the AC field dependence of different heterostructure variants at 183 K to elucidate the orientation difference [Figs. 3(e) and 3(f)]. The dielectric response of the (001)- and the (111)-oriented PMN heterostructures are similar; however, domain-wall response only occurs in the (111)- but not the (001)-oriented BZT heterostructures, which confirms that the substrate clamping in the (111)-oriented heterostructure stabilizes the nanoscale-polar structure and

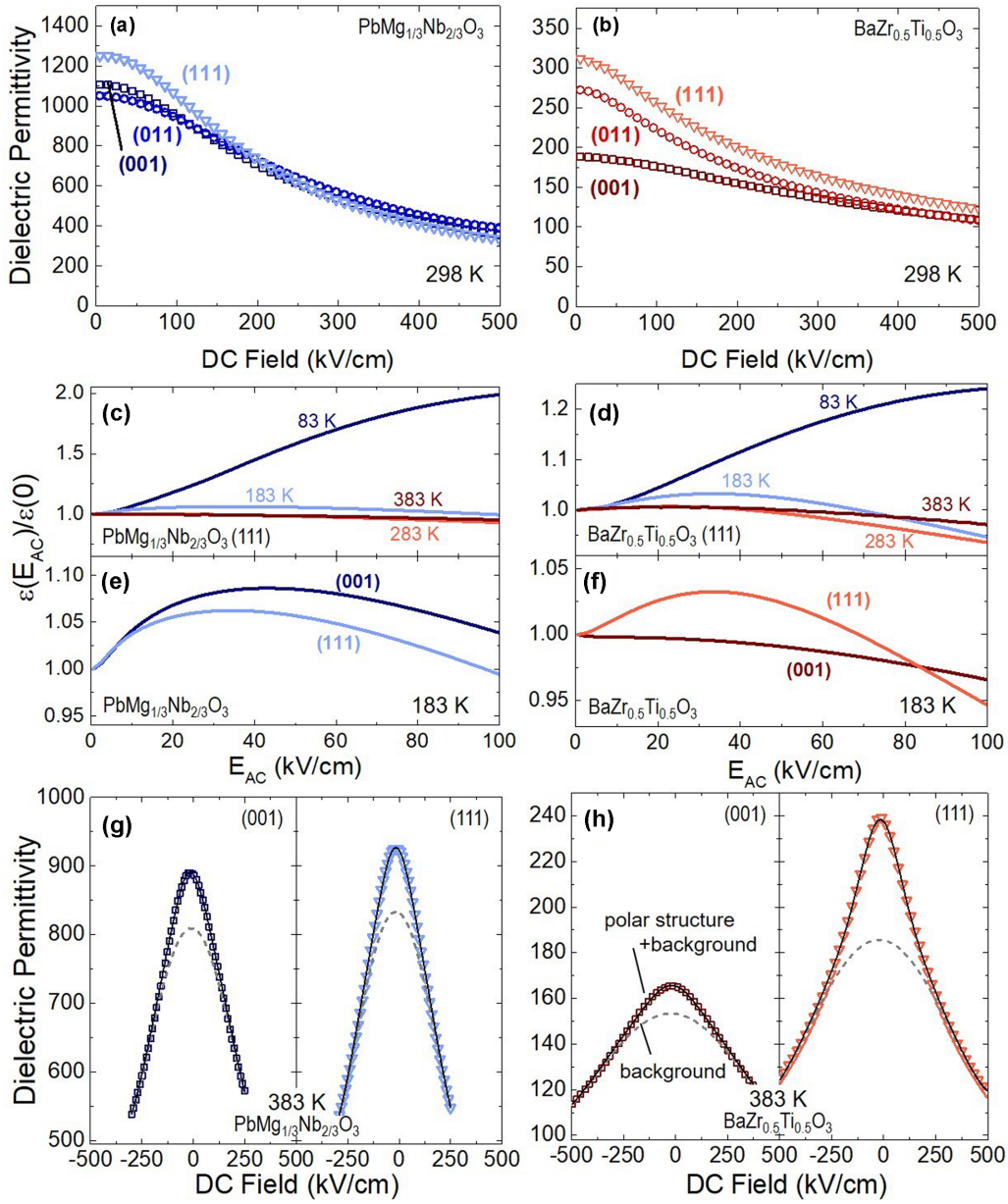

FIG. 3. Out-of-plane dielectric permittivity measured as function of DC field (at 10 kHz and 298 K) for the (a) PMN and (b) BZT heterostructures. Dielectric nonlinearity measured as a function of AC field at 83, 183, 283, and 383 K for (111)-oriented (c) PMN and (d) BZT heterostructures. Comparison of the dielectric nonlinearity measured as a function of AC field (at 183 K) for (001)- and (111)-oriented heterostructures of (e) PMN and (f) BZT. Comparison between the dielectric tunability at 383 K for (001)- and (111)-oriented heterostructures of (g) PMN and (h) BZT. Data points show the experimental data. Fits to the theoretical model reveal two different contributions to the dielectric response: dashed lines show the background contribution and solid lines show the sum of both the polar-structure contribution and the background contribution.

preserves the domain-wall response to a higher temperature. This observation is consistent with the enhanced remnant polarization and elevated critical temperatures in the (111)-oriented heterostructures.

The weak interaction between the nanoscale-polar structures at 383 K allows us to further probe the dielectric response from reorientation of the nanoscale-polar structures. We measured the dielectric permittivity as a function of DC bias at 383 K [Figs. 3(g) and 3(h)] and Supplemental Material, Fig. S8 [33]) and to extract information about the individual polar structures, we fit the dielectric permittivity-DC field data to a model describing nanoscale-polar structure reorientation, which was originally proposed to analyze the dielectric response across the ferroelectric phase transition in Ca-doped $SrTiO_3$ [49] and paraelectric $KTaO_3$ [50]. Assuming that the reorientation of each nanoscale-polar structure is independent, then the nanoscale-polar structure contribution to the permittivity (ε_p) has the form

$$\varepsilon_p(E_{DC}) = \frac{Np^2}{\varepsilon_0 k_B T}\cosh^{-2}\frac{pE_{DC}}{k_B T}, \quad (1)$$

TABLE II. Summary of fitting parameters to the dielectric tunability curves at 383 K [Figs. 3(g) and 3(h) and Supplemental Material, Fig. S8]. p and N denote the average dipole moment and the number density of the nanoscale-polar structures, respectively.

	p ($\times 10^{-20}$ μC cm)	N ($\times 10^{19}$ cm^{-3})
PMN (001)	5.23	1.39
PMN (011)	5.18	1.41
PMN (111)	5.23	1.60
BZT (001)	3.28	0.54
BZT (011)	3.88	1.36
BZT (111)	4.02	1.53

where E_{DC} denotes the bias field, N is the number density of nanoscale-polar structures, p is their average dipole moment, and T is the temperature. The background contribution to the permittivity (ε_b) can also be expressed in a polynomial form as

$$\varepsilon_b(E_{DC}) = \varepsilon_1 - \varepsilon_2 E_{DC}^2 + \varepsilon_3 E_{DC}^4 + o\left(E_{DC}^6\right). \quad (2)$$

Here, we limit the polynomial to the fourth order [49,50], and fit the dielectric permittivity-DC field data. The experimental data fit well with the model [Figs. 3(g) and 3(h)] and Supplemental Material, Fig. S8 [33]). The N and p values of the nanoscale-polar structures are summarized (Table II), and are of the same order of magnitude as the values previous reported for PMN thin films [51]. The PMN heterostructures have (nearly) identical p values and exhibit a variation in N of just 15% going from (001)- to (111)-oriented heterostructures. In contrast, p increases by 23% and N by 183% as one transitions from (001)- to (111)-oriented BZT heterostructures.

These results suggest that substrate clamping in the (111)-oriented heterostructures facilitates both the nucleation and growth of nanoscale-polar structures, while clamping in the (001)-oriented heterostructure does not. Also, the effect is strong for the homovalent relaxor BZT but weak for the heterovalent relaxor PMN. As another piece of information, the orientational difference of BZT is not diminished in relatively thick films, which indicates that the clamping effect is significant across the film, instead of limited to the film-substrate interface (Supplemental Material, Fig. S11 [33]). We propose that the constraints from substrate clamping partially suppress the random elastic field and distort the energy landscape in the thin films, thus favoring dipoles pointing out of the plane over ones pointing in the plane. If the out-of-plane direction lies along the polar axis, as in the (111)-oriented heterostructures, the distortion of the energy landscape favors having the dipoles aligned along the polar axis, and promotes the alignment of nearby dipoles, which results in the nucleation and growth of nanoscale-polar structures. If the out-of-plane direction does not lie along a polar axis, as in the (001)-oriented heterostructures, the alignment of dipoles along the out-of-plane direction is energetically unfavored, and the nucleation or growth of nanoscale-polar structures is not promoted. Considering the elastic nature of the random field in a homovalent relaxor such as BZT, the random field can be effectively suppressed by elastic clamping. In contrast, for a heterovalent relaxor such as PMN, even if the random elastic field is suppressed, the random electric field helps to preserve the polar (dis)order, resulting in a relative insensitivity to elastic clamping. As a consequence, the homovalent relaxor BZT exhibits a strong orientation dependence for the dielectric permittivity and critical temperatures, which is not observed in the heterovalent relaxor PMN.

An alternative interpretation for the observations, however, might attribute the strength of orientation dependence to differences in the flatness of the free-energy landscape, which is inherent in the relaxor material and unrelated to the substrate, in the different materials. Specifically, if the free-energy wells along the polar axes are deeper and the free-energy barriers in between are higher in BZT than in PMN, a sharper contrast between the dielectric properties measured along different crystallographic directions would be observed. Note that this effect would occur in both in-plane and out-of-plane directions; that is, the in-plane measurements along the [100] and [110] would reveal dielectric anisotropy to a similar extent as observed in the out-of-plane measurements on (001)- and (011)-oriented heterostructures. To determine which interpretation is more favorable, we conducted an additional experiment which compares the dielectric properties measured along the in-plane [100] and [110] on the (001)-oriented heterostructures of both BZT and PMN (Fig. 4). It is noted that both BZT and PMN show minimal anisotropy between measurements along the in-plane [100] and [110], which indicates that the free-energy landscape is relatively flat in both materials. Thus, the flatness of the energy landscape is unlikely to fully explain the strength of the orientation dependence, which suggests that the orientation dependence is likely to originate from clamping instead of an inherent anisotropy in the material.

The discrepancy between the in-plane and out-of-plane dielectric response further consolidates the observations of strong clamping effects. The (001)-oriented PMN heterostructures show a small difference (27%) between the in-plane and out-of-plane directions [Fig. 4(a)]. Considering that the dielectric response is isotropic in bulk, single-crystal PMN [52], the relatively preserved isotropy in the epitaxial thin films suggests that the energy landscape in PMN is not severely distorted even when clamped onto a substrate. The (001)-oriented BZT heterostructures, on the other hand, reveal a much larger discrepancy between the in-plane and out-of-plane directions (45%) [Fig. 4(b)]. It is further noted that the discrepancy between the out-of-plane and the in-plane dielectric response is negligible at high temperatures where the nanoscale-polar structures become unstable, reinforcing the idea that the background contribution is isotropic. Thus, the anisotropy must come from the nanoscale-polar structure contribution. Near the peak in the dielectric permittivity, the strong anisotropy indicates that substrate clamping suppresses the out-of-plane response relative to the in-plane response. Again, we propose that substrate clamping constrains and aligns the nanoscale-polar structures, where reorientation is frustrated and only small rotations or extensions of local dipoles are allowed. Supposing that the nanoscale-polar structures have an average out-of-plane polarization, an anisotropy will be induced between the out-of-plane and the in-plane directions, similar to the anisotropy in classic ferroelectrics with large domains [53]. The large anisotropy in the BZT

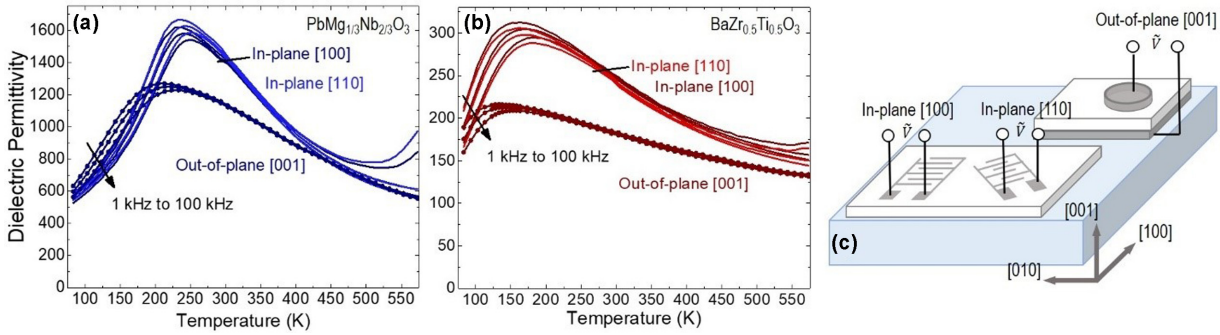

FIG. 4. Comparison of the dielectric permittivity as a function of temperature measured along the in-plane [100], in-plane [110], and out-of-plane [001] on (001)-oriented (a) PMN and (b) BZT heterostructures. (c) A diagram of the device structures for in-plane and out-of-plane dielectric measurements. In-plane measurements are performed on interdigital electrodes (IDEs), while out-of-plane measurements were carried out on circular capacitors.

heterostructures thus results from the clamping effect and serves as another piece of evidence of its high sensitivity to substrate clamping.

Finally, we discuss the implications of these observations to material choice in thin-film applications. The current work suggests that PMN exhibits a relatively weaker effect from substrate clamping and thus is likely a more attractive option for thin-film applications. In addition, PMN shows minimal orientation dependence, which alleviates the need for epitaxial thin films and allows for the use of polycrystalline films. BZT, on the other hand, shows a large orientation dependence and requires specific orientations to maximize its response, thus likely limiting its potential for some applications. The comparison between PMN and BZT indicates that the random-field characteristics in relaxor materials strongly affects the susceptibility to substrate clamping. In heterovalent relaxors, random electric fields are important, and hence the polar structure is insensitive to clamping, while in homovalent relaxors, only random elastic fields exist, and hence the polar structure is more susceptible to clamping. Thus, when considering potential relaxor materials for next-generation thin-film applications, one might consider the use of or search for relaxor materials with large random electric fields and small random elastic fields as a pathway to reduce the sensitivity to clamping, and enhance the performance of relaxor thin films.

IV. CONCLUSION

All told, this work provides a comparative study of substrate clamping effects in (001)-, (011)-, and (111)-oriented PMN and BZT heterostructures. While the PMN heterostructures exhibit a negligible orientation dependence and a small anisotropy between the out-of-plane and in-plane properties, the BZT heterostructures show a large orientation dependence in dielectric permittivity and critical temperatures, accompanied by a large anisotropy between the out-of-plane and in-plane responses. The observed difference between the PMN and BZT heterostructures is attributed to the different origins of random fields. The random elastic field in the homovalent relaxor BZT can be suppressed when the film is elastically clamped to the substrate, while the random electric field in the heterovalent relaxor PMN preserves (to some extent) the relaxor nature and reduces the sensitivity to clamping. In homovalent relaxors, substrate clamping promotes the alignment of dipoles and facilitates the nucleation and growth of nanoscale-polar structures, which is not observed in heterovalent relaxors. The relative insensitivity to clamping in the PMN thin films is desired for thin-film devices and hints at the possibility of designing future relaxor materials with strong random electric fields to reduce clamping effect. Ultimately, these results indicate that the random-field characteristics are influential for relaxor properties, and could act as a tuning parameter in future material designs.

ACKNOWLEDGMENTS

Z.T. acknowledges the support of the Army Research Office under Grant No. W911NF-21-1-0118. J.K. acknowledges support of the Army Research Office under Grant No. W911NF-21-1-0126. A.F. acknowledges support from the National Science Foundation under Grant No. DMR-1708615. L.W.M. acknowledges support from the ARL/ARO Collaborative for Hierarchical Agile and Responsive Materials (CHARM) under Cooperative Agreement No. W911-NF-19-2-0119.

[1] S. Zhang, F. Li, X. Jiang, J. Kim, J. Luo, and X. Geng, Advantages and challenges of relaxor-$PbTiO_3$ ferroelectric crystals for electroacoustic transducers–A review, Prog. Mater. Sci. **68**, 1 (2015).

[2] S.-E. Park and T. R. Shrout, Ultrahigh strain and piezoelectric behavior in relaxor based ferroelectric single crystals, J. Appl. Phys. **82**, 1804 (1997).

[3] J. Kim, S. Saremi, M. Acharya, G. Velarde, E. Parsonnet, P. Donahue, A. Qualls, D. Garcia, and L. W. Martin, Ultrahigh capacitive energy density in ion-bombarded relaxor ferroelectric films, Science **369**, 81 (2020).

[4] H. Pan, F. Li, Y. Liu, Q. Zhang, M. Wang, S. Lan, Y. Zheng, J. Ma, L. Gu, Y. Shen *et al.*, Ultrahigh–energy density lead-free

dielectric films via polymorphic nanodomain design, Science **365**, 578 (2019).

[5] S. Pandya, J. Wilbur, J. Kim, R. Gao, A. Dasgupta, C. Dames, and L. W. Martin, Pyroelectric energy conversion with large energy and power density in relaxor ferroelectric thin films, Nat. Mater. **17**, 432 (2018).

[6] T. Correia, J. Young, R. W. Whatmore, J. Scott, N. Mathur, and Q. Zhang, Investigation of the electrocaloric effect in a $PbMg_{2/3}Nb_{1/3}O_3$-$PbTiO_3$ relaxor thin film, Appl. Phys. Lett. **95**, 182904 (2009).

[7] A. Mischenko, Q. Zhang, R. W. Whatmore, J. Scott, and N. Mathur, Giant electrocaloric effect in the thin film relaxor ferroelectric $0.9\,PbMg_{2/3}Nb_{1/3}O_3$–$0.1PbTiO_3$ $PbTiO_3$ near room temperature, Appl. Phys. Lett. **89**, 242912 (2006).

[8] C.-B. Eom and S. Trolier-McKinstry, Thin-film piezoelectric MEMS, MRS Bull. **37**, 1007 (2012).

[9] J. Irwin, S. Lindemann, W. Maeng, J. J. Wang, V. Vaithyanathan, J. M. Hu, L. Q. Chen, D. G. Schlom, C. B. Eom, and M. S. Rzchowski, Magnetoelectric coupling by piezoelectric tensor design, Sci. Rep. **9**, 19158 (2019).

[10] A. Fernandez, J. Kim, D. Meyers, S. Saremi, and L. W. Martin, Finite-size effects in lead scandium tantalate relaxor thin films, Phys. Rev. B **101**, 094102 (2020).

[11] J. C. Frederick, T. H. Kim, W. Maeng, A. A. Brewer, J. P. Podkaminer, W. Saenrang, V. Vaithyanathan, F. Li, L. Q. Chen, D. G. Schlom, and S. Trolier-McKinstry, Visualization of dielectric constant-electric field-temperature phase maps for imprinted relaxor ferroelectric thin films, Appl. Phys. Lett. **108**, 132902 (2016).

[12] V. Nagarajan, C. S. Ganpule, B. Nagaraj, S. Aggarwal, S. P. Alpay, A. L. Roytburd, E. D. Williams, and R. Ramesh, Effect of mechanical constraint on the dielectric and piezoelectric behavior of epitaxial $PbMg_{2/3}Nb_{1/3}O_3$ (90%)–$PbTiO_3$(10%) relaxor thin films, Appl. Phys. Lett. **75**, 4183 (1999).

[13] R. Keech, S. Shetty, M. A. Kuroda, X. H. Liu, G. J. Martyna, D. M. Newns, and S. Trolier-McKinstry, Lateral scaling of $PbMg_{2/3}Nb_{1/3}O_3$-$PbTiO_3$ thin films for piezoelectric logic applications, J. Appl. Phys. **115**, 234106 (2014).

[14] R. Keech, L. Ye, J. L. Bosse, G. Esteves, J. Guerrier, J. L. Jones, M. A. Kuroda, B. D. Huey, and S. Trolier-McKinstry, Declamped piezoelectric coefficients in patterned 70/30 lead magnesium niobate–lead titanate thin films, Adv. Funct. Mater. **27**, 1605014 (2017).

[15] V. Nagarajan, A. Roytburd, A. Stanishevsky, S. Prasertchoung, T. Zhao, L.-Q. Chen, J. Melngailis, O. Auciello, and R. Ramesh, Dynamics of ferroelastic domains in ferroelectric thin films, Nat. Mater. **2**, 43 (2003).

[16] S. S. Hong, J. H. Yu, D. Lu, A. F. Marshall, Y. Hikita, Y. Cui, and H. Y. Hwang, Two-dimensional limit of crystalline order in perovskite membrane films, Sci. Adv. **3**, eaao5173 (2017).

[17] G. Dong, S. Li, M. Yao, Z. Zhou, Y. Q. Zhang, X. Han, Z. Luo, J. Yao, B. Peng, Z. Hu *et al.*, Super-elastic ferroelectric single-crystal membrane with continuous electric dipole rotation, Science **366**, 475 (2019).

[18] D. Pesquera, E. Parsonnet, A. Qualls, R. Xu, A. J. Gubser, J. Kim, Y. Jiang, G. Velarde, Y. L. Huang, H. Y. Hwang *et al.*, Beyond substrates: Strain engineering of ferroelectric membranes, Adv. Mater. **32**, 2003780 (2020).

[19] A. Bokov and Z.-G. Ye, Recent progress in relaxor ferroelectrics with perovskite structure, J. Mater. Sci. **41**, 31 (2006).

[20] D. Viehland, S. Jang, L. E. Cross, and M. Wuttig, Freezing of the polarization fluctuations in lead magnesium niobate relaxors, J. Appl. Phys. **68**, 2916 (1990).

[21] L. E. Cross, Relaxor ferroelectrics, Ferroelectrics **76**, 241 (1987).

[22] H. Takenaka, I. Grinberg, S. Liu, and A. M. Rappe, Slush-like polar structures in single-crystal relaxors, Nature (London) **546**, 391 (2017).

[23] V. Westphal, W. Kleemann, and M. Glinchuk, Diffuse Phase Transitions and Random-Field-Induced Domain States of the "Relaxor" Ferroelectric $PbMg_{2/3}Nb_{1/3}O_3$, Phys. Rev. Lett. **68**, 847 (1992).

[24] V. V. Shvartsman and D. C. Lupascu, Lead-free relaxor ferroelectrics, J. Am. Ceram. Soc. **95**, 1 (2012).

[25] C. Laulhé, A. Pasturel, F. Hippert, and J. Kreisel, Random local strain effects in homovalent-substituted relaxor ferroelectrics: A first-principles study of $BaTi_{0.74}Zr_{0.26}O_3$, Phys. Rev. B **82**, 132102 (2010).

[26] Z.-G. Ye and H. Schmid, Optical, dielectric and polarization studies of the electric field-induced phase transition in $PbMg_{2/3}Nb_{1/3}O_3$ [PMN], Ferroelectrics **145**, 83 (1993).

[27] A. Bokov, M. Maglione, and Z.-G. Ye, Quasi-ferroelectric state in $Ba(Ti_{1-x}Zr_x)O_3$ relaxor: Dielectric spectroscopy evidence, J. Phys.: Condens. Matter **19**, 092001 (2007).

[28] C. Filipič, Z. Kutnjak, R. Pirc, G. Canu, and J. Petzelt, $BaZr_{0.5}Ti_{0.5}O_3$: Lead-free relaxor ferroelectric or dipolar glass, Phys. Rev. B **93**, 224105 (2016).

[29] P. Sciau, G. Calvarin, and J. Ravez, X-ray diffraction study of $BaTi_{0.65}Zr_{0.35}O_3$ and $Ba_{0.92}Ca_{0.08}Ti_{0.75}Zr_{0.25}O_3$ compositions: Influence of electric field, Solid State Commun. **113**, 77 (1999).

[30] S. Prosandeev, D. Wang, A. Akbarzadeh, B. Dkhil, and L. Bellaiche, Field-induced Percolation of Polar Nanoregions in Relaxor Ferroelectrics, Phys. Rev. Lett. **110**, 207601 (2013).

[31] Z. Kutnjak, B. Vodopivec, and R. Blinc, Anisotropy of electric field freezing of the relaxor ferroelectric $PbMg_{2/3}Nb_{1/3}O_3$, Phys. Rev. B **77**, 054102 (2008).

[32] I.-K. Jeong, T. Darling, J. Lee, T. Proffen, R. Heffner, J. Park, K. Hong, W. Dmowski, and T. Egami, Direct Observation of the Formation of Polar Nanoregions in $PbMg_{2/3}Nb_{1/3}O_3$, Using Neutron Pair Distribution Function Analysis, Phys. Rev. Lett. **94**, 147602 (2005).

[33] See Supplemental Material at http://link.aps.org/supplemental/10.1103/PhysRevB.105.094107 for additional characterization of the samples used in this study, including additional x-ray diffraction and electrical characterization, which includes Refs. [54–58].

[34] V. Buscaglia, S. Tripathi, V. Petkov, M. Dapiaggi, M. Deluca, A. Gajović, and Y. Ren, Average and local atomic-scale structure in $BaZr_xTi_{1-x}O_3$ (x = 0.10, 0.20, 0.40) ceramics by high-energy x-ray diffraction and Raman spectroscopy, J. Phys.: Condens. Matter **26**, 065901 (2014).

[35] Y. M. Jin, Y. U. Wang, A. G. Khachaturyan, J. Li, and D. Viehland, Conformal Miniaturization of Domains with Low Domain-Wall Energy: Monoclinic Ferroelectric States near the Morphotropic Phase Boundaries, Phys. Rev. Lett. **91**, 197601 (2003).

[36] S. Bhattacharyya, J. R. Jinschek, H. Cao, Y. U. Wang, J. Li, and D. Viehland, Direct high resolution transmission electron

microscopy observation of tetragonal nanotwins within the monoclinic Mc phase of $Pb(Mg_{1/3}Nb_{2/3})O_3$–$0.35PbTiO_3$ crystals, Appl. Phys. Lett. **92**, 142904 (2008).

[37] A. Kumar, J. N. Baker, P. C. Bowes, M. J. Cabral, S. Zhang, E. C. Dickey, D. L. Irving, and J. M. LeBeau, Atomic-resolution electron microscopy of nanoscale local structure in lead-based relaxor ferroelectrics, Nat. Mater. **20**, 62 (2021).

[38] C. Laulhé, F. Hippert, R. Bellissent, A. Simon, and G. Cuello, Local structure in $BaZr_xTi_{1-x}O_3$ relaxors from neutron pair distribution function analysis, Phys. Rev. B **79**, 064104 (2009).

[39] G. Burns and F. Dacol, Crystalline ferroelectrics with glassy polarization behavior, Phys. Rev. B **28**, 2527 (1983).

[40] B. Dkhil, P. Gemeiner, A. Al-Barakaty, L. Bellaiche, E. Dul'kin, E. Mojaev, and M. Roth, Intermediate temperature scale T* in lead-based relaxor systems, Phys. Rev. B **80**, 064103 (2009).

[41] J. Toulouse, The three characteristic temperatures of relaxor dynamics and their meaning, Ferroelectrics **369**, 203 (2008).

[42] A. Levstik, Z. Kutnjak, C. Filipič, and R. Pirc, Glassy freezing in relaxor ferroelectric lead magnesium niobate, Phys. Rev. B **57**, 11204 (1998).

[43] A. A. Bokov and Z.-G. Ye, Dielectric relaxation in relaxor ferroelectrics, J. Adv. Dielectr. **2**, 1241010 (2012).

[44] B. Vugmeister and H. Rabitz, Dynamics of interacting clusters and dielectric response in relaxor ferroelectrics, Phys. Rev. B **57**, 7581 (1998).

[45] A. Glazounov and A. Tagantsev, A "breathing" model for the polarization response of relaxor ferroelectrics, Ferroelectrics **221**, 57 (1999).

[46] R. Xu, J. Karthik, A. R. Damodaran, and L. W. Martin, Stationary domain wall contribution to enhanced ferroelectric susceptibility, Nat. Commun. **5**, 3120 (2014).

[47] S. Hashemizadeh and D. Damjanovic, Nonlinear dynamics of polar regions in paraelectric phase of $(Ba_{1-x}, Sr_x)TiO_3$ ceramics, Appl. Phys. Lett. **110**, 192905 (2017).

[48] A. Tagantsev and A. Glazounov, Mechanism of polarization response in the ergodic phase of a relaxor ferroelectric, Phys. Rev. B **57**, 18 (1998).

[49] U. Bianchi, J. Dec, W. Kleemann, and J. Bednorz, Cluster and domain-state dynamics of ferroelectric $Sr_{1-x}Ca_xTiO_3$ ($x = 0.007$), Phys. Rev. B **51**, 8737 (1995).

[50] C. Ang, A. Bhalla, and L. Cross, Dielectric behavior of paraelectric $KTaO_3$, $CaTiO_3$, and $(Ln_{1/2}Na_{1/2})TiO_3$ under a dc electric field, Phys. Rev. B **64**, 184104 (2001).

[51] M. Tyunina, J. Levoska, K. Kundzinsh, and V. Zauls, Polar state in epitaxial films of the relaxor ferroelectric $PbMg_{1/3}Nb_{2/3}O_3$, Phys. Rev. B **69**, 224101 (2004).

[52] X. Zhao, W. Qu, X. Tan, A. Bokov, and Z.-G. Ye, Electric field-induced phase transitions in (111)-, (110)-, and (100)-oriented $Pb(Mg_{1/3}Nb_{2/3})O_3$ single crystals, Phys. Rev. B **75**, 104106 (2007).

[53] M. Davis, M. Budimir, D. Damjanovic, and N. Setter, Rotator and extender ferroelectrics: Importance of the shear coefficient to the piezoelectric properties of domain-engineered crystals and ceramics, J. Appl. Phys. **101**, 054112 (2007).

[54] D. Viehland, S. Jang, L. Eric Cross, and M. Wuttig, The dielectric relaxation of lead magnesium niobate relaxor ferroelectrics, Philos. Mag. (Abingdon) **64**, 335 (1991).

[55] A. Glazounov, A. Tagantsev, and A. Bell, Evidence for domain-type dynamics in the ergodic phase of the $PbMg_{1/3}Nb_{2/3}O_3$ relaxor ferroelectric, Phys. Rev. B **53**, 11281 (1996).

[56] G. W. Farnell, I. A. Cermak, P. Silvester, and S. Wong, Capacitance and field distributions for interdigital surface-wave transducers, IEEE Trans. Sonics Ultrason. **17**, 188 (1969).

[57] D. Dimos, M. Raymond, R. Schwartz, H. Al-Shareef, and C. Mueller, Tunability and calculation of the dielectric constant of capacitor structures with interdigital electrodes, J. Electroceram. **1**, 145 (1997).

[58] S. Prosandeev, D. Wang, and L. Bellaiche, Properties of Epitaxial Films Made of Relaxor Ferroelectrics, Phys. Rev. Lett. **111**, 247602 (2013).